

Four-wave mixing in microstructure fiber

Jay E. Sharping, Marco Fiorentino, Ayodeji Coker, and Prem Kumar

Center for Photonic Communication and Computing, Department of Electrical and Computer Engineering, Northwestern University,
2145 North Sheridan Road, Evanston, Illinois 60208-3118

Robert S. Windeler

Bell Laboratories, Lucent Technologies, 700 Mountain Avenue, Murray Hill, New Jersey 070974

Received March 8, 2001

We report what we believe to be the first experimental demonstration of nondegenerate four-wave mixing in a microstructure fiber. The effect of the $\chi^{(3)}$ nonlinearity is enhanced in such a fiber because of the small core area, and we achieve phase matching by operating near the zero-dispersion wavelength (≈ 750 nm). We have observed parametric gains of more than 13 dB in 6.1-m-long fiber with a pump peak power of only 6 W. We compare our experimental gain results with those predicted by theory and explore the effects of Raman shift and (or) amplification and cascaded nonlinear mixing. © 2001 Optical Society of America

OCIS codes: 060.2320, 060.4370, 190.4380, 190.4970.

Recently, much excitement has been generated over the application of microstructure fibers¹ (MFs) in nonlinear optics.² The generation of a supercontinuum in a 1-m-long MF by use of femtosecond pulses has proved that the nonlinear response can be quite dramatic.³ One expects to be able to observe in MFs all the nonlinear effects that are present in standard optical fibers. The ability to combine a small core area with single-mode behavior over a wide wavelength range and with engineerable dispersion characteristics suggests that one can take greater advantage of the relatively weak $\chi^{(3)}$ nonlinearity of glass in MFs.

It is well known that four-wave mixing (FWM) can be phase matched in the vicinity of the zero-dispersion wavelength (λ_0) of an optical fiber.⁴ This has been demonstrated for standard telecommunication fibers⁵ as well as dispersion-shifted fibers.⁶ At visible wavelengths, polarization modulation instability was demonstrated in single-mode fiber by use of variable birefringence to adjust the gain profile.⁷ Zhang *et al.*⁸ have also reported FWM in the visible by achieving phase matching through a combination of self- and cross-phase modulation. In recent experiments, our group has used widely tunable fiber-optic parametric devices for optical communication applications, where the device operation is based on the FWM gain.⁹

In this Letter we report on our experiments with controlled FWM in a MF. We demonstrate achieving nondegenerate parametric gain over a 30-nm range of pump wavelengths near the λ_0 of the MF. A comparison of the observed gain behavior with quasi-cw FWM theory allows us to confirm our theoretical understanding of the mechanism at play and to evaluate the wavelength dependence of the group-velocity dispersion (GVD) coefficient of the MF near λ_0 . Since the dispersion characteristics of these fibers can be adjusted during the fabrication process, our experiment demonstrates the potential for the use of MFs in broadband parametric amplifiers, wavelength shifters, and other optical communication devices. Another goal of our project is to demonstrate twin-beam quantum correlations

in the signal and idler beams generated through FWM¹⁰ in MFs to create a fiber-based source of polarization-entangled photon pairs near the 800-nm wavelength. Such a source could then be combined with Bell-state measurements to become part of an integrated quantum computing and communication scheme.¹¹

The theory of FWM in optical fibers has been explored fully by Stolen and Bjorkholm¹³ and is summarized along with experimental results by Agrawal.⁴ One obtains the following coupled amplitude equations that describe FWM in the fiber:

$$\frac{\partial A_1}{\partial z} = -\frac{\alpha}{2} A_1 + i\gamma(|A_1|^2 A_1), \quad (1)$$

$$\begin{aligned} \frac{\partial A_{2(3)}}{\partial z} = & -\frac{\alpha}{2} A_{2(3)} + i\gamma[(2|A_1|^2)A_{2(3)} \\ & + A_1^2 A_{3(3)}^* \exp(i\Delta k z)]. \end{aligned} \quad (2)$$

In Eqs. (1) and (2), A_1 , A_2 , and A_3 are the field amplitudes of the pump, signal, and idler (conjugate) beams, respectively, and α is the attenuation coefficient of the fiber according to $P(z) = P(0)\exp(-\alpha z)$, where P is power and z is propagation distance. The nonlinear coefficient, γ , is related to the nonlinear refractive index, n_2 , by $\gamma = n_2\omega_1/A_{\text{eff}}c$, where A_{eff} is the effective mode area of the field and ω_1 is the angular frequency of the pump. The phase mismatch is given by $\Delta k = 2k_1 - k_2 - k_3$, where k_1 , k_2 , and k_3 are the wave-vector magnitudes for the pump, signal, and idler beams, respectively. In Eqs. (1) and (2) we have assumed that the pump is much stronger than the input signal and that group-velocity mismatch among the three beams is not significant; these are reasonable assumptions for the experiments described in this Letter. The effects of linear loss and self- and cross-phase modulation are included, however. The phase-matching condition is

$$\kappa = 2\gamma P_1 + \Delta k \approx 2\gamma P_1 + \beta(\omega_2 - \omega_1)^2 = 0, \quad (3)$$

where β is the GVD coefficient at ω_1 and ω_2 is the angular frequency of the signal beam. The GVD

parameter, D , is often used instead of β , and they are related by $D = -\beta 2\pi c/\lambda^2$. When a strong pump interacts with a weak signal under phase-matching conditions, one observes amplification of the signal beam as well as generation of an idler beam of angular frequency ω_3 according to $\omega_3 = 2\omega_1 - \omega_2$. The primary factors influencing the FWM gain within the fiber are the nonlinear coefficient γ , the pump power, the fiber length, and the GVD coefficient β . By operating above the λ_0 of a fiber, one can achieve $\beta < 0$, which, in addition to a small amount of pump self-phase modulation, results in $\kappa \approx 0$ as required by Eq. (3).

The experimental setup used to demonstrate phase-matched FWM in MF is shown in Fig. 1. The pump and the input signal pulses are derived from a 75-MHz train of 150-fs-duration pulses emitted by a mode-locked Ti:sapphire laser (Coherent Model Mira 900). The laser beam is directed onto a diffraction grating, and a short- and a long-wavelength slice of the spectrum are coupled into separate optical fibers. This coupling creates two synchronous beams with 3–5-nm wavelength separation, with the center wavelength tunable over a 720–850-nm range. Autocorrelation measurements of the two pulse trains indicate that they are well described by a Gaussian shape with FWHM $\Delta t \approx 2.1$ ps and FWHM spectral width $\Delta\lambda \approx 0.8$ nm, corresponding to a time–bandwidth product of 0.89. According to these measurements, the maximum peak power of our pulses is ≈ 12 W. The two synchronous beams are then recombined via a 90/10 coupler and injected into the MF. The pump and the signal's optical paths are adjusted to yield temporal overlap in the MF, and their polarizations are aligned by fiber polarization controllers. The polarization state at the input to the MF is set by use of a polarization beam-splitter cube and a half-wave plate. Control over the input polarization state is critical because the MF is birefringent owing to its elliptical core. Birefringence, however, works in our favor because when the pump and the signal are injected along one of the principal axes the polarization state is maintained as the beams propagate through the fiber, allowing the largest component of the $\chi^{(3)}$ nonlinearity to be active. The MF used in these experiments was fabricated at Bell Labs, Lucent Technologies.³ It consists of an ~ 1.7 - μm -diameter silica core surrounded by a hexagonal array of ~ 1.4 - μm -diameter air voids. The attenuation coefficient, α , was measured to be 0.02 m^{-1} (86 dB/km) by comparison of the insertion losses for two different MF lengths. Quantitative measurements of the FWM behavior were made with an optical spectrum analyzer.

Figure 2 shows a typical FWM optical spectrum at the output of a 6.1-m-long MF. Here we used a strong pump beam at 753 nm and a weak signal beam at 758 nm. The spectrum shows the undepleted pump, the amplified signal, and the generated idler at 747 nm. There is some spectral overlap between the tail of the pump and the amplified signal. Therefore, an accurate determination of the FWM gain, G , requires that the pump contribution be subtracted

according to $G = (P_{as} - P_p)/P_{us}$, where P_{us} , P_{as} , and P_p are the power spectral densities of the unamplified signal, the amplified signal, and the pump, respectively, at the signal wavelength.

The spectra in Fig. 2 clearly show that large gain is achievable for a pump-to-signal spacing of 5 nm. Gain values of more than 20 (13 dB) were obtained in a reproducible way in our setup. Note that if standard dispersion-shifted fiber is used for FWM in the 1550-nm region, a fiber length of 225 m would be needed,¹⁰ as can be verified by use of $A_{\text{eff}} = 50.3 \mu\text{m}^2$ in the simulations described below. We were able to observe FWM, albeit with limited gain, in fibers as short as 1 m in length. We were also able to tune the signal as much as 12 nm away from the pump and still observe mixing between the beams.

Figure 3 shows plots of the FWM gain, measured from spectra like those in Fig. 2, versus peak pump power for various pump wavelengths ranging from 743 to 770 nm. Fits to the numerical solutions of Eqs. (1) and (2) are also shown. A central-difference space-stepping method was employed, and periodic boundary conditions were implemented. The GVD coefficient, D , was used as a fitting parameter. Other fiber parameters treated as constants in the numerical

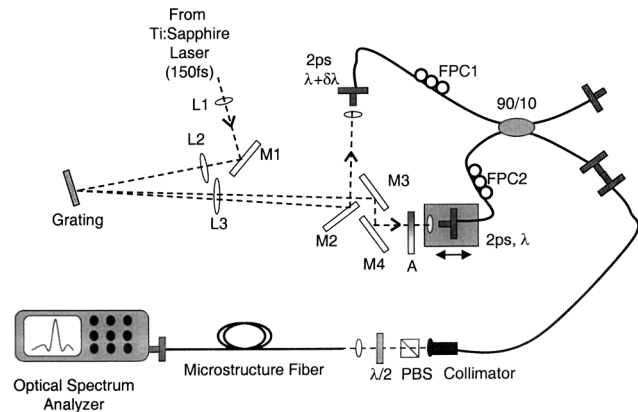


Fig. 1. Schematic of the experimental setup used to investigate FWM in MFs. L1–L3, lenses; M1–M4, mirrors; A, attenuator; FPC1, FPC2, fiber polarization controllers; PBS, polarization beam splitter; $\lambda/2$, half-wave plate.

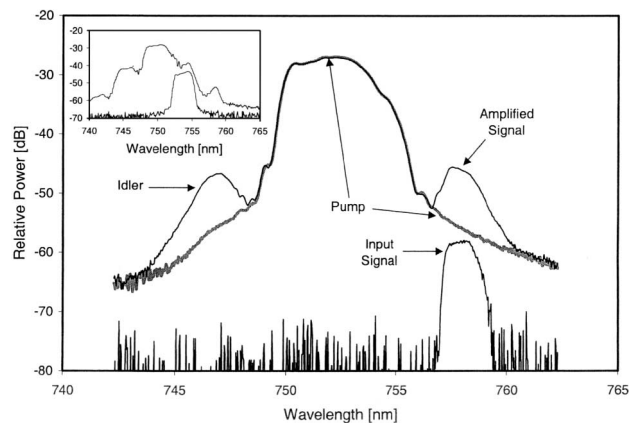


Fig. 2. Typical FWM spectrum observed at the output of the MF. The inset shows a spectrum in which higher-order cascaded mixing is evident.

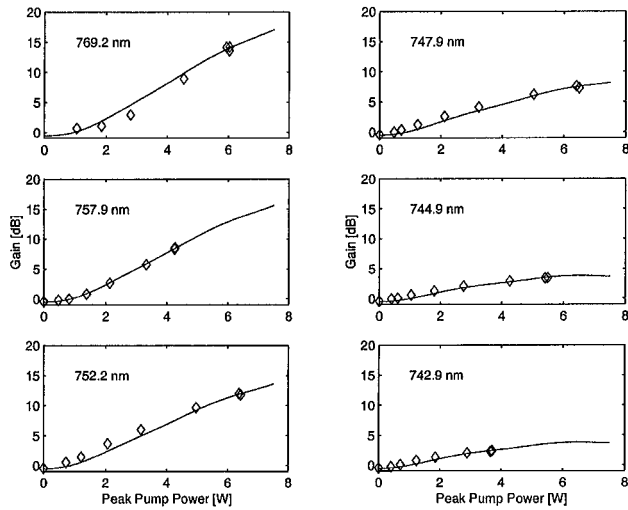


Fig. 3. Plots of FWM gain versus peak pump power for several different pump wavelengths. The diamonds represent experimental data, and the curves are fits to Eqs. (1) and (2).

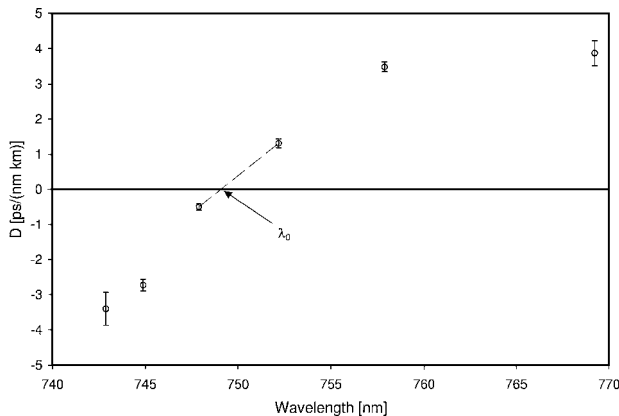


Fig. 4. Plot of the GVD coefficient, D , as a function of wavelength, showing λ_0 of the MF under test. The error bars represent a 95% confidence interval for D , resulting from the fits shown in Fig. 3.

solution were $n_2 = 2.8 \times 10^{-20} \text{ m}^2/\text{W}$, $\alpha = 0.02 \text{ m}^{-1}$, and $A_{\text{eff}} = 2.4 \mu\text{m}^2$. The input pump and signal were taken to be Gaussian-shaped pulses of 2.1 ps FWHM. The nonlinear coefficient and the effective core area are consistent with those obtained previously for this fiber.³ The value of α used in the simulations was obtained from our loss measurements as described above. Based on the results of the fits in Fig. 3, we obtain the GVD coefficient, D , which is plotted in Fig. 4 as a function of the pump wavelength. The value for λ_0 , read directly from this graph, is 749 nm, which is somewhat different from the 767-nm value reported earlier for this fiber.³ The discrepancy is perhaps due to variations in the core size and air-fill fraction along the fiber that is introduced during fabrication.

Raman shifts and (or) amplification, cascaded (higher-order) mixing, and supercontinuum generation could also be observed with our setup. The peak of the Raman-gain spectrum is $\approx 10 \text{ THz}$ from the pump,⁴ which corresponds to $\approx 19 \text{ nm}$ for these

wavelengths. We minimized the Raman effect in our FWM measurements by narrowing the spectra of the pump and the signal to a few nanometers FWHM and keeping the signal wavelength close to that of the pump (within 5–7 nm). Careful analysis of our data indicates that there is a small amount of Raman amplification, but it is generally negligible compared with the FWM gain. By adjusting the signal power and its spectral separation from the strong pump beam, we are able to see the onset of cascaded mixing (see the inset in Fig. 2). As the input signal power is increased, it acts along with the original pump and the generated idler to create a new peak at a slightly longer wavelength than the others. Each new peak stimulates mixing and generates additional peaks, which build up symmetrically with respect to the pump wavelength, eventually forming a continuum.¹³ We minimize these effects in our FWM-gain measurements by injecting a signal that is weak enough and setting the signal wavelength at least 5 nm from the pump.

In conclusion, we have demonstrated nondegenerate four-wave mixing in a microstructure fiber and confirmed that the behavior is consistent with theory. We believe this to be the first demonstration of controlled FWM in these novel-structure fibers. The results demonstrate the feasibility of a number of potential applications for MFs, including generation of quantum-correlated photon pairs for quantum optics and their use as active devices for optical communications.

This research was supported in part by the U.S. Army Research Office under grants DAAD19-00-1-0177 and DAAD19-00-1-0469 (e-mail address: j-sharping@northwestern.edu).

References

1. J. C. Knight, T. A. Birks, P. St. J. Russell, and D. M. Atkin, *Opt. Lett.* **21**, 1547 (1996).
2. N. G. R. Broderick, T. M. Monro, P. J. Bennett, and D. J. Richardson, *Opt. Lett.* **24**, 1395 (1999).
3. J. K. Ranka, R. S. Windeler, and A. J. Stentz, *Opt. Lett.* **25**, 25 (2000).
4. G. P. Agrawal, *Nonlinear Fiber Optics*, 2nd ed. (Academic, San Diego, Calif., 1995).
5. W. Washio, K. Inoue, and S. Kishida, *Electron. Lett.* **16**, 658 (1980).
6. D. K. Serkland and P. Kumar, *Opt. Lett.* **24**, 92 (1999).
7. S. G. Murdoch, R. Leonhardt, and J. D. Harvey, *Opt. Lett.* **20**, 866 (1995).
8. J. Zhang, Q. Li, W. Pan, S. Y. Luo, and Y. L. Chen, *Opt. Lett.* **26**, 214 (2001).
9. Y. Su, L. Wang, A. Agarwal, and P. Kumar, *Opt. Commun.* **184**, 151 (2000).
10. J. E. Sharping, M. Fiorentino, and P. Kumar, *Opt. Lett.* **26**, 367 (2001).
11. D. Bouwmeester, A. Ekert, and A. Zeilinger, *The Physics of Quantum Information* (Springer-Verlag, Berlin, 2000).
12. R. H. Stolen and G. D. Bjorkholm, *IEEE J. Quantum Electron.* **18**, 1062 (1982).
13. K. R. Tamura, H. Kubota, and M. Nakazawa, *IEEE J. Quantum Electron.* **36**, 773 (2000).